[Title Page]

Effect of flame surface area of downward propagating flames induced by single and double laser irradiation on transition to parametric instability

Nguyen Truong Gia Tri[1], Ajit Kumar Dubey[1,2,3], Nozomu Hashimoto[1], Osamu Fujita[1]

[1] Division of Mechanical and Space Engineering, Hokkaido University,

Kita 13 Nishi 8, Kita-ku, Sapporo, 060-8628, Japan

[2] RACMaS - Research Alliance Center for Mathematical Sciences, Tohoku University 6-3 Aoba, Aramaki, Aoba-ku, Sendai, Miyagi, 980-8578, Japan

[3] Institute of Fluid Science, Tohoku University, 2-1-1 Katahira, Aoba-ku, Sendai, Miyagi, 980-8578, Japan

Corresponding author information:

Osamu Fujita*

Professor, Hokkaido University,

Kita 13 Nishi 8, Kita-ku, Sapporo, 060-8628, Japan

E-mail address: ofujita@eng.hokudai.ac.jp

Tel.: +81-11-706-6385; Fax: +81-11-706-7841

[Title Page]

Tables

[Title Page]

Figures

1. Schematics of the experimental setup.
2. Still images of typical downward-propagating flame behaviors in the tube without laser irradiation (mixture compositions are given in Table 1).
3. Flame propagation behavior induced by *SLI* and *DLI* under various total laser powers (mixture compositions are given in Table 1).
4. An illustration of the concave structure deformation process of the flame induced by *DLI*.
5. Pressure fluctuations of the conditions shown in Fig. 3.
6. Critical laser power required for the transition under various laminar burning velocities (mixture compositions are given in Table 1).
7. Stability diagram at S_L =16 cm/s for $C_2H_4/O_2/CO_2$ mixture with Le = 1.05.
8. Acoustic pressure fluctuation in the tube during flame propagation under various conditions (mixture compositions are given in Table 1).
9. Relationship between $(ak)^2$ of the concave structure and the growth rate of acoustic pressure fluctuation at S_L = 13 cm/s and Le = 1.05. The horizontal dotted line denotes the growth rate without laser irradiation. The horizontal dashed line denotes the critical growth rate (~ 0.400 1/s) to reach parametric instability.
10. Relationship between the concave segment area and the growth rate of acoustic pressure fluctuation at S_L = 13 cm/s and Le = 1.05. The horizontal dotted line denotes the growth rate without laser irradiation. The horizontal and vertical dashed lines denote the critical growth rate (~ 0.400 1/s) and the critical average concave segment area (~ 5 cm^2), respectively, to reach parametric instability.
11. Amplitude and wavelength of concave structures induced by *SLI* and *DLI* at S_L = 13 cm/s.
12. Relationship between the deformed convex area and the growth rate of acoustic pressure fluctuation at S_L = 12 cm/s and Le = 0.8.

13. Comparison of the growth of the acoustic pressure fluctuation among no laser, *SLI*, and *DLI* for S_L = 12 cm/s and *Le* = 0.8.

Effect of flame surface area of downward propagating flames induced by single and double laser irradiation on transition to parametric instability

Nguyen Truong Gia Tri, Ajit Kumar Dubey, Nozomu Hashimoto, Osamu Fujita*

Division of Mechanical and Space Engineering, Hokkaido University,

Kita 13 Nishi 8, Kita-ku, Sapporo, 060-8628, Japan

Abstract

The single laser irradiation (*SLI*) method was adopted to develop a double laser irradiation (*DLI*) method to investigate the effects of laser-induced structures of downward-propagating flames in a tube on the transition from primary acoustic instability to parametric instability. Previously, the *SLI* method was effectively used to study the interaction between acoustic oscillation and flame structure by controlling the shape of the flame front. The deformed cellular structure (either concave or convex) of the *SLI*-induced flame can transition from primary acoustic instability to parametric instability under certain conditions. We conducted experiments in the same combustion tube with $C_2H_4/O_2/CO_2$ mixtures using both *SLI* and *DLI* for comparison. The *DLI* method forms double cellular structures, while *SLI* only forms single cellular structures on the flames. It was found that the DLI method was more effective than SLI in generating transition to parametric instability under same total laser power. Furthermore, a linear relationship was found between the area of the deformed structure (irrespective of its dimension) and the corresponding growth rate of acoustic pressure fluctuation during the propagation of the deformed flame. *SLI*- and *DLI*-induced deformed structures having the same deformed surface area demonstrate the same growth rate of thermo-acoustic instability regardless of the difference in $(ak)^2$, where a is the amplitude and k is the wavenumber of the deformed structures, respectively. This factor described in the velocity coupling mechanism is important to reveal the growth rate of thermo-acoustic instability due to the variation in the flame surface area. The results revealed that the actual flame surface area, rather than $(ak)^2$ of the laser-induced downward-

propagating flame structure, determines the transition in the presence of nonhomogeneous cell distribution induced by *SLI* and *DLI*. The total deformed surface area is a more comprehensive criterion for transition to parametric instability.

---

* Corresponding author: Tel.: +81-11-706-6385. E-mail address: ofujita@eng.hokudai.ac.jp

Keywords: Parametric instability, Double laser irradiation method, Flame structures, Diffusive-thermal instability

1. Introduction

Thermo-acoustic instabilities are often destructive to the operation of various combustion systems and are major challenge in the development of lean premixed combustors with ultra-low emissions. Thermo-acoustic instabilities have their origin in the complex dynamic coupling between the self-generated acoustic waves and the heat release fluctuations from the flame. Rayleigh [1] stated in his famous Rayleigh criterion that acoustic oscillation can be amplified if the acoustic pressure and the heat release fluctuations are in phase. Numerous researches have been conducted to understand the mechanisms of the thermo-acoustic instabilities. Of these, a simple experiment to generate and study thermo-acoustic instabilities is a downward-propagating flame in an open-closed tube. In its simplest form, the combustion chamber can also be considered as a tube in which acoustic oscillations can be sustained. Additionally, longitudinal acoustic modes can be formed in the tube in which the acoustic energy is a sinusoidal function of the position of the tube. Accordingly, a downward-propagating flame interacts with a wide range of self-generated acoustic oscillations in the tube. At particular positions of the flame in the tube, the flame starts to oscillate and amplify the acoustic modes of the tube, then thermo-acoustic instabilities can be observed. The instabilities mechanism could be considered equivalent to thermoacoustic instabilities mechanisms that may lead to strong discrete-frequency oscillations in combustion chambers of modern gas turbines.

Flames propagating in tubes can spontaneously produce acoustic oscillation. In a classical study of thermo-acoustic instabilities in a tube, Searby [2] has experimentally observed two distinct acoustic instabilities under specific flame structures in a tube. For a slow flame, a primary acoustic instability occurs corresponding to a flat flame oscillation. As the flame speed increases, the primary acoustic instability rapidly transitions to violent parametric instability, producing a vibrating cellular flame and leading to turbulent flame. This parametric instability of the flame front is triggered only by preexisting finite-amplitude acoustic oscillations. At the onset of this instability, the flat flame becomes cellular with smaller corrugated cells oscillating at half of the acoustic excitation frequency. The wavenumbers of the corrugated structures and the acoustic velocity amplitude can be predicted using theoretical

methods [3,4]. The flame propagation speed and the amplitude of the pressure oscillations are significantly higher during parametric instability as compared to those in primary acoustic instability. Finally, the amplitude of the cells increases until a turbulent combustion regime occurs. Even though many works present parametric instability in propagating flame experiments, this instability has also been observed in burner stabilized premixed flames in tubes [3]. In principle, this instability can also occur in gas turbine combustion process if the amplitudes of existing oscillations are high enough for onset of parametric instability. In such cases, very high amplitude oscillations can be generated. These instabilities observed in the experiments of Searby [2] were also found in methane–air flames propagating through the annulus of a Taylor–Couette burner [5,6]. Dubey et al. [7] analytically and experimentally studied the effect of geometric parameters on thermo-acoustic instabilities and found that velocity coupling mechanism is the dominant mechanism. However, pressure coupling can also be important when flame area does not change during flame propagation [8]. A critical diameter was also found at which the stronger parametric instability can be generated in mixtures with lowest laminar burning velocity [8]. The higher acoustic modes of the parametric instability can also be generated in gaseous fuels which has been experimentally and theoretically studied [9].

Essentially velocity coupling mechanism is related to the change in flame area which modulates the heat release to influence thermoacoustic instabilities. Pelce and Rochwerger [10] have theoretically derived a transfer function for velocity coupling mechanism used to define the growth rate of the thermo-acoustic instability driven by the acoustic acceleration of weak cellular flame front ($ak << 1$, a is amplitude and k is wavenumber of the cellular flame). Clanet [11] extended the calculation for realistic flame with higher aspect ratio of coupling parameters, ak, and the results were in good agreement with the experiment on propane–air flames. The effect of velocity coupling can be studied more precisely if we can control the flame structure. The flame structure can be changed by changing the combustible mixture and geometry [7]. Another way is by modifying the flame shape artificially by irradiating the flame with a laser beam. In previous studies, the CO_2 laser irradiation method was extensively used to artificially control the flame shape. The laser energy, which is absorbed by the

unburnt mixture, is negligible compared to the energy release of the flame. Hence, laser irradiation is used to generate specific deformed structures on the flame without significantly modifying the mixture's combustion properties. This method is a new experimental approach to study the interaction of flame structure and acoustic field. Specifically, this method has been utilized to study the onset of primary acoustic instability [12,13], the effect of Lewis number (*Le*) on the generation of thermo-acoustic instability [14,15] and the mechanism of generation of parametric instability in a laser-irradiated flame [16,17]. Chung et al. [18] recently established a criteria map of the transition from primary acoustic instability to parametric instability when the flame curvature under different *Le* is controlled by external CO_2 laser irradiation. However, these studies use the single laser irradiation (*SLI*) method. When the flat flame is exposed to a single CO_2 laser beam, a single cellular structure is formed. In this work, we developed a double laser irradiation (*DLI*) method based on the *SLI* setup. *DLI* has a similar flame deformation process with that of the *SLI* setup but generates double cellular structures on the flame. As a spatially sinusoidal shape is formed, the geometry of the cellular structures is characterized by the amplitude of the cell (a) and wavenumber (k) as a function of wavelength, $k = 2\pi/\lambda$. At a given S_L and using the same total laser power, *SLI* and *DLI* induce different coupling parameters for deformed cellular flames. Consequently, flames exposed to *SLI* and *DLI* generate different thermo-acoustic responses. These responses can be comparatively examined to develop a more comprehensive criterion for the transition from primary acoustic instability to parametric instability.

This paper presents a comparative experimental investigation on dynamics of downward-propagating flames exposed to *SLI* and *DLI*. The structure of the laser-induced flames and their effect on the growth of acoustic pressure fluctuations are discussed to clarify the criteria of the transition from primary acoustic instability to parametric instability.

2. Experimental setup and procedure

The experiments were performed in a vertical combustion tube with for *SLI* and *DLI*, as shown in Fig. 1. The combustion tube was a 705-mm-long transparent acrylic tube with a 50-mm inner diameter.

The tube was open at the upper end and closed at the bottom end during experiments. A mechanism including electromagnets and springs was used to automatically open the top lid triggered by an external command at the beginning of ignition. $C_2H_4/O_2/CO_2$ mixture was filled into the tube through a small inlet with a valve. Table 1 lists the properties and compositions of gas mixtures. The effect of the Lewis number (*Le*) on the transition at $Le = 0.8$ and $Le = 1.05$ (treated as $Le > 1$) has been clarified in [18]. Thus, this study uses the same gas mixtures with $Le = 1.05$ used in [18]. The laminar burning velocity, S_L, of the gas mixtures was calculated using CHEMKIN (PREMIX) with a detailed chemical mechanism USC II [19]. In a typical experiment, the tube was flushed with premixed gases at atmospheric pressure and ambient temperature for few minutes while the top lid was closed. The valve was then closed, and the mixture was allowed to become uniformly quiescent. Consequently, the top lid was opened, and the mixture was immediately ignited by a spark plug installed near the top end of the tube. Hence, the combustion took place under one open end and another closed end boundary condition. A high-speed camera (FASTCAM Mini UX100 recording at 1000 fps) was used to record the downward-propagating flame. The pressure fluctuation of the unburnt mixture during flame propagation was measured by a pressure sensor (PCB Piezotronics) flush mounted at the bottom end. Each experiment is repeated at least six times and excellent reproducibility is observed. Here, we have presented a representative experiment for each case.

Figure 1 shows a schematic of both *SLI* (Fig. 1a) and *DLI* setups (Fig. 1b) and how they are guided into the combustion tube. The *SLI* setup included a CO_2 laser generator (SYNRAD Firestar v20; beam diameter, 3.3 mm; and wavelength, 10.6 mm), focusing lenses, a mechanical shutter, and a mirror (Mirror 1). The shutter was placed in the laser path to control the timing of laser irradiation. Yellow ZnSe windows were attached to the top lid and bottom of the tube to enable the passing of the CO_2 laser beam(s) along and through the tube. A CO_2 laser was used because it can be absorbed by C_2H_4 presented in the test mixture [20]. It is therefore assumed that only the unburnt mixture absorbs the laser energy. The *DLI* setup was configured by adding an optical arrangement to the *SLI* setup. The added arrangement consisted of a plate beam splitter and another mirror (Mirror 2). The beam splitter

was set at a 45° angle to the incidence beam to separate it into a reflected and a transmitted beam at 50:50 ratio (tolerance of 3%). Mirror 2 was set below the beam splitter to fold the optical path of reflected laser beam by 90° making it parallel to the transmitted laser beam. Consequently, two spitted laser beams were collimated and then directed into the tube due to the normal reflection in mirror 1. The beam separation was set to 18 mm. Note that the only difference between the *DLI* and *SLI* setups was the additional optical arrangement. In the *DLI* experiment, the double laser beam was created by splitting the single laser beam from the *SLI* setup, making the results collected using the two setups comparable. Moreover, the power of the laser beam(s) from *SLI* and *DLI* was measured to ensure comparable results between *SLI* and *DLI* experiments. The maximum laser power used in this experiment was 12 W. The laser was irradiated 0.8 s after the ignition and slightly before the appearance of the flat flame in experiments. The flame was continuously exposed to laser irradiation for 3 s to allow the deformed structure to propagate through the middle region of the tube where maximum growth rate of thermo-acoustic instability is usually observed [9,10].

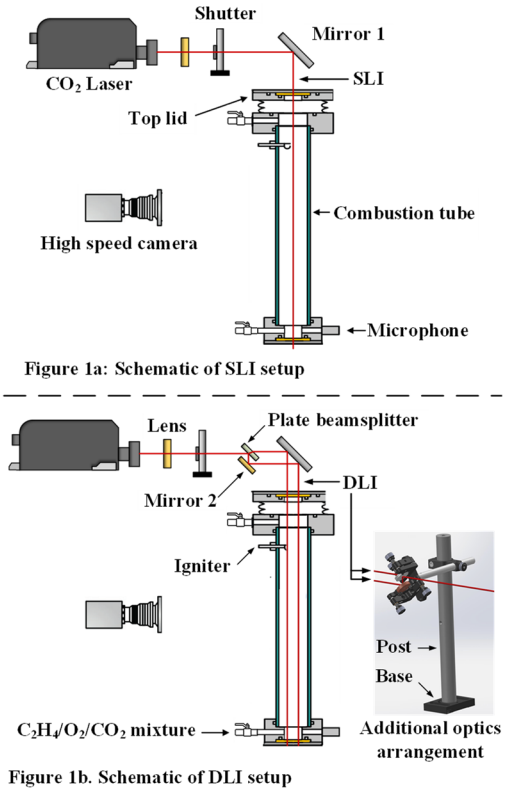

Fig. 1. Schematics of the experimental setup.

Table 1. Composition and properties of experimental gas mixtures with $Le > 1$.

C_2H_4 [%]	O_2 [%]	CO_2 [%]	Φ	Le	S_L [cm/s]
5.445	20.418	74.137	0.8	1.05	10
5.893	22.098	72.009			13
6.007	22.525	71.468			14
6.119	22.945	70.936			15
6.232	23.334	70.434			16

Table 2. Composition and properties of experimental gas mixtures with $Le < 1$.

C_2H_4 [%]	O_2 [%]	CO_2 [%]	Φ	Le	S_L [cm/s]
7.780	19.447	72.773	1.2	0.8	12

3. Results and discussion

3.1. Observation of the downward-propagating flame induced by laser irradiation

Figure 2 shows three different regimes of downward-propagating flames without laser irradiation. The regime depends on laminar burning velocity, S_L. (I) For S_L below 11 cm/s, the flame propagates with a curved shape generated by hydrodynamic instability and produces no sound. (II) For S_L in the range of 12–15 cm/s, a flat flame developed from the curved flame oscillates in an acoustic field generated by the primary acoustic instability. (III) For S_L above 15 cm/s, parametric instability follows primary acoustic instability. Due to parametric instability, a corrugated structure appears on the vibrating flat flame which eventually breaks into turbulent flame. These regimes are qualitatively similar to those reported in previous work [2,4,9] which also show typical pressure traces associated with various regimes.

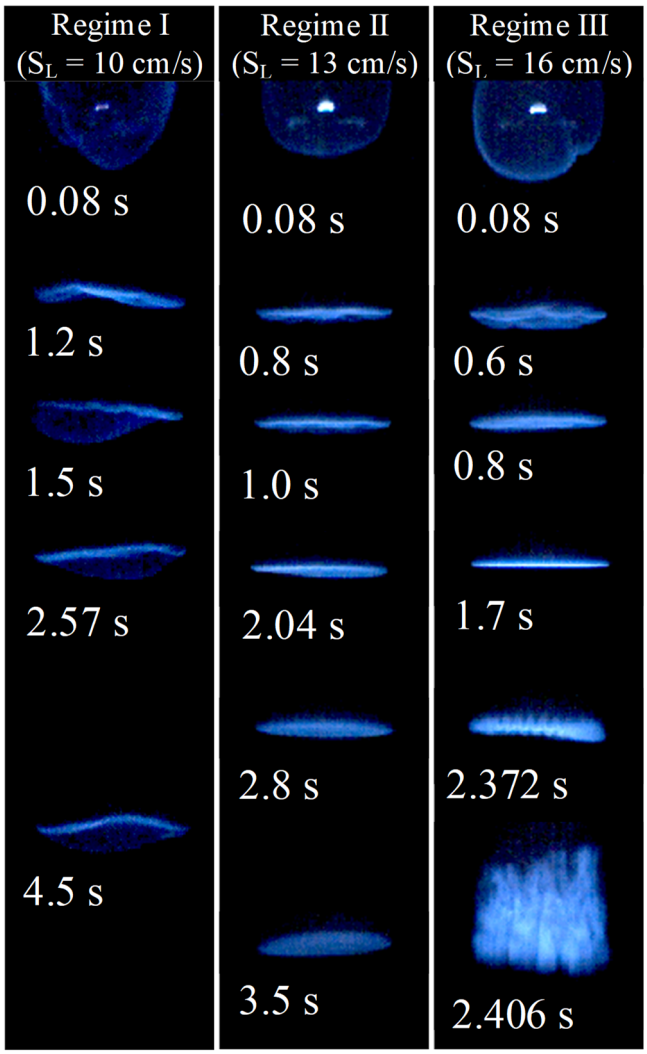

Fig. 2. Still images of typical downward-propagating flame behaviors in the tube without laser irradiation (mixture compositions are given in Table 1).

Thereafter, the flat flame in regime II was selected as the default flame for experiments with CO_2 laser irradiation because the flat flame is observed for a larger part of flame propagation during regime II. The laser could help the flat flame to generate a transition to parametric instability as in regime III but without increasing S_L. Due to the constant structure and surface area, the flat part that remined after laser irradiation had a limited contribution on driving to the transition. Hence, the instability increment compared to that without laser irradiation is attributed to the propagation behavior of the deformed part of the flame. This consideration enables a clear description of the effect of laser irradiation on the transition criteria. The experiments could also be performed by selecting I as default case but it would require much larger laser power than II.

Figure 3 illustrates the experimental flame images depicting sequential behaviors of the default flames induced by *SLI* and *DLI*. In general, the flame behaviors induced by *SLI* and *DLI* are qualitatively similar. Figure 4 illustrates the flame deformation process for *DLI* case for easier understanding. Figure 5 shows the pressure fluctuation associated with the conditions shown in Fig. 3. Chung et al. [18] described the deformation of flames and their transition to parametric instability induced by *SLI*. Following the incidence of the laser beam, a portion of the unburnt mixture just before the flame front was preheated along the laser path. As a result, the flame temperature was locally increased and the local burning velocity was downwardly enhanced at the center of the flame. The flame front was then deformed toward the unburnt mixture and formed a convex structure. Consequently, the thermal-diffusive effect comes into play as the gradient of temperature and species concentration are no longer parallel to the average direction of flame propagation. For a flame with $Le > 1$, due to the dominance of thermal diffusion over species diffusion, the convex flame front tends to be stabilized. Thus, the transition to parametric instability from the convex flame requires a higher laser power compared with the flame with a lower *Le*. On the other hand, the laser irradiation simultaneously decreases the density of the unburnt mixture along the laser path and the generation of upward flow induced by the buoyancy effect. With a laser exposure of 3 s, the strength of buoyancy-driven flow becomes significant and overcomes the evolution of the convex structure to establish a concave structure. This deformed concave flame continues to propagate and generates the transition to parametric instability with sufficient laser power. In addition, the concave structure formation has been previously described in [21].

From Fig. 4, it can be seen that double concave structure was developed from the initial double convex structure along the two laser paths, and it further initiated the transition at a critical laser power. As described above, a large single cellular structure or a smaller double concave structure can be artificially induced from the flat flame using *SLI* or *DLI* at the same total laser power. It can be seen that the amplitude of the concave structure is lower with *DLI* than that with *SLI* because the amount of energy added by laser heating is halved for each beam at the same total laser power. As shown in

Fig. 3, 10 W of laser power used in the *SLI* setup cannot drive the transition to parametric instability, but it does in the case of *DLI*. Therefore, the different flame structures induced by *SLI* and *DLI* methods lead to the difference in critical laser power at which the transition occurs. Clearly, the total laser power is not the criterion to generate the transition to parametric instability from a flat flame, and flame dynamics generated by *SLI* and *DLI* needs to be further clarified. The transition from primary acoustic instability to parametric instability is recognized by the onset of the corrugated structure and followed by a sudden increase in the amplitude of acoustic pressure compared to that in the primary acoustic instability region as shown in Fig. 5. All the conditions shown in Fig. 5 demonstrated this sudden acoustic pressure increment in the parametric instability region, except for the case of *SLI* at S_L = 13 cm/s, 10 W laser power.

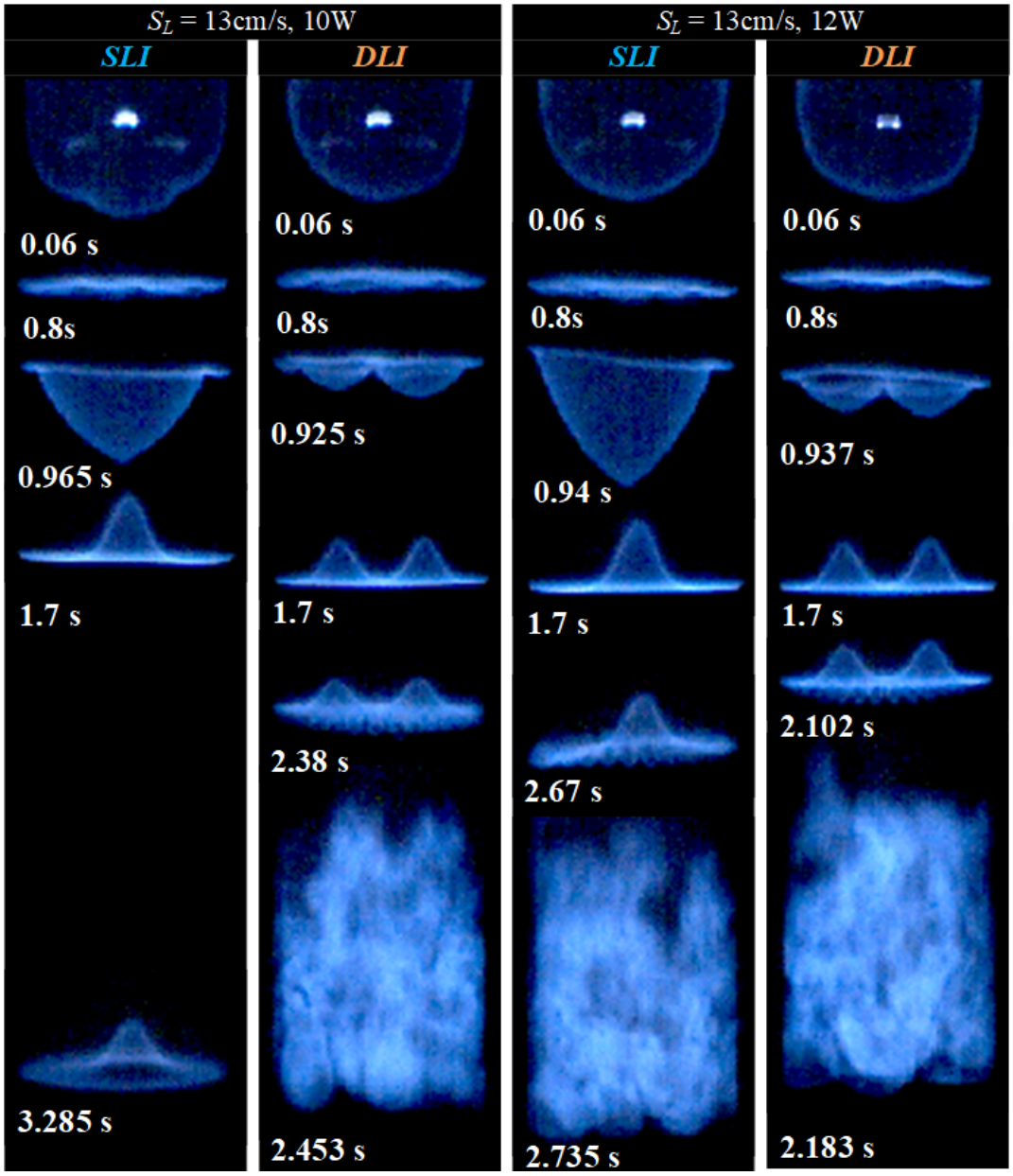

Fig. 3. Flame propagation behavior induced by *SLI* and *DLI* under various total laser powers (mixture compositions are given in Table 1).

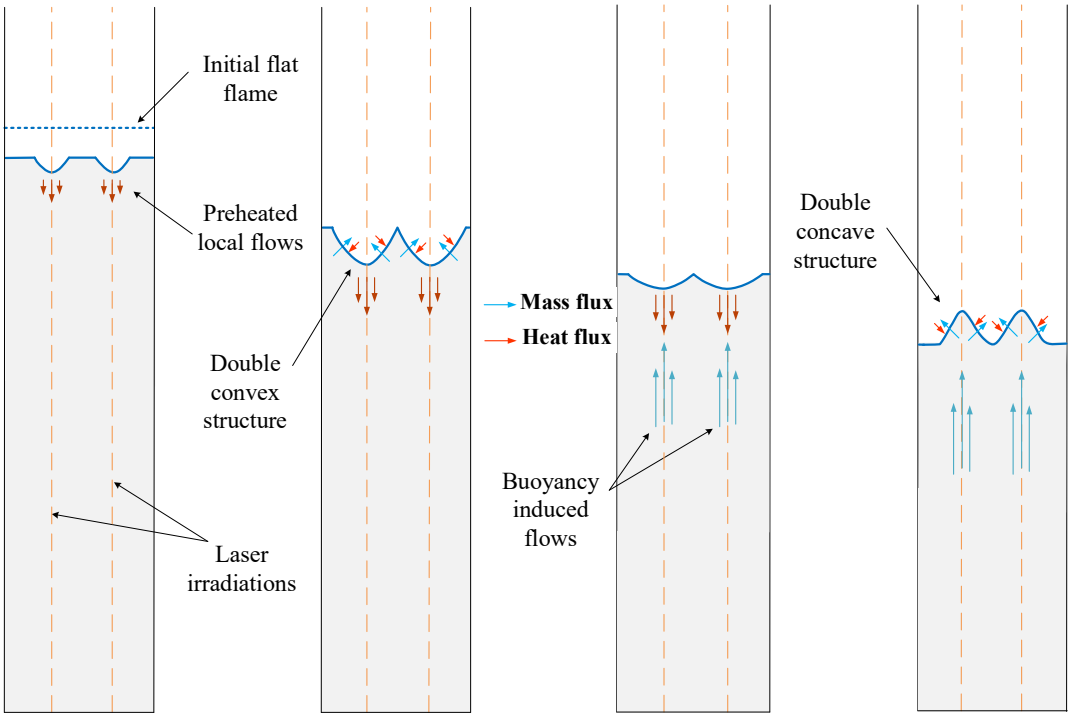

Fig. 4. An illustration of the concave structure deformation process of the flame induced by *DLI*.

Figure 6 shows critical laser power, which is the minimum total laser power required to induce the transition to parametric instability from the flat flame for a range of S_L from 13 cm/s to 16 cm/s. For *DLI*, the horizontal axis denotes the total power of the two laser beams in the *DLI* setup or the power of a single beam in the *SLI* case. At S_L = 16 cm/s, transition occurs without laser irradiation (i.e., the critical laser power is 0 W). When S_L < 16 cm/s, transition occurs only with laser irradiation for the deformed concave flame. Figure 6 shows that the minimum laser power required for generating the transition of the flame reduces as S_L increases which is understandable because by increasing S_L we are moving closer to the onset of regime III where parametric instability is generated without any laser irradiation. Importantly, at a given S_L, *DLI* triggered the transition using a lower laser power compared to *SLI*. This result indicates that the flame deformation by *DLI* is more effective than that by *SLI* in causing the transition from primary acoustic instability to parametric instability at the same total laser power. Consequently, the flame structure and pressure history generated by the *SLI* and *DLI* were further analyzed to understand the factors controlling the transition to parametric instability.

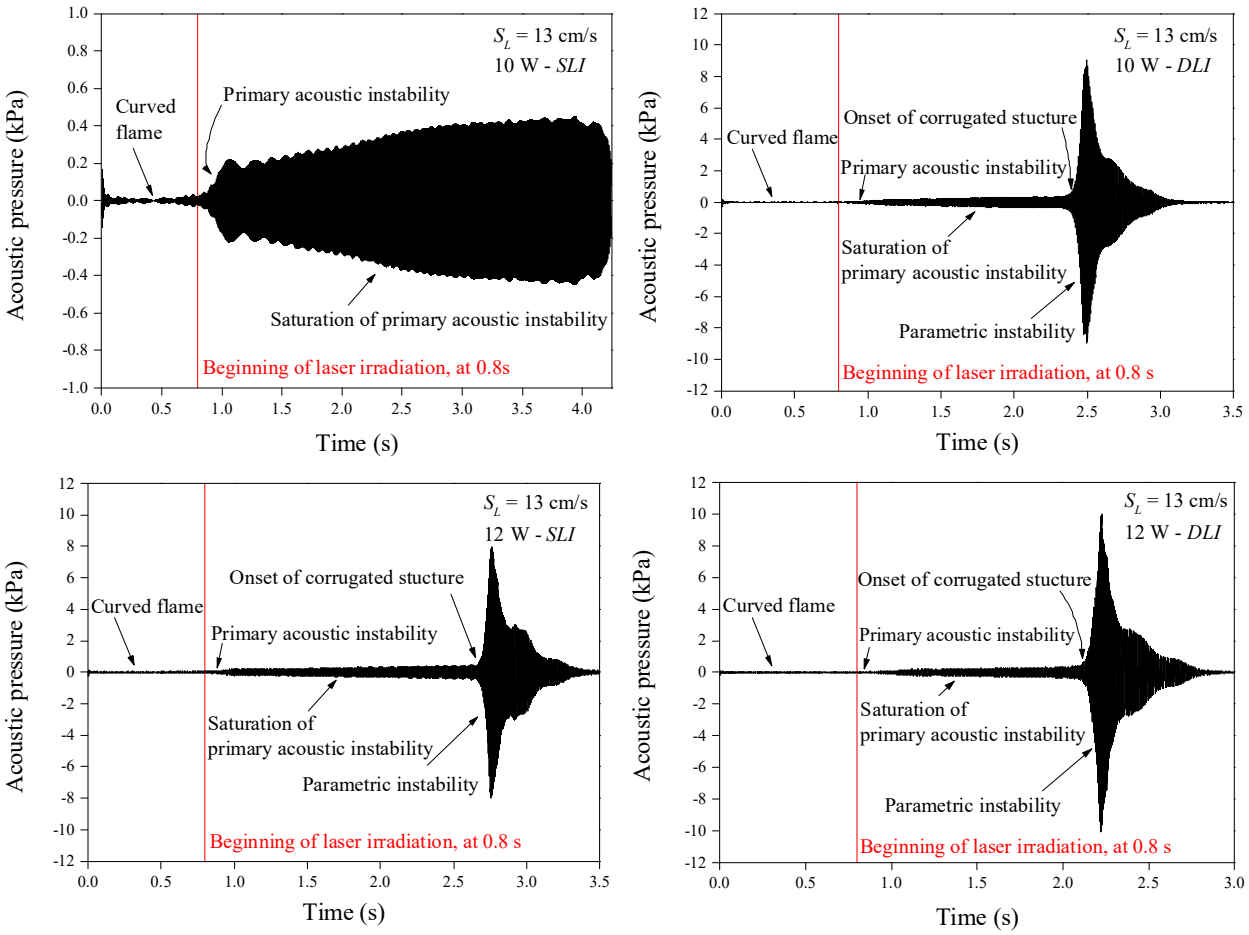

Fig. 5. Pressure fluctuations of the conditions shown in Fig. 3.

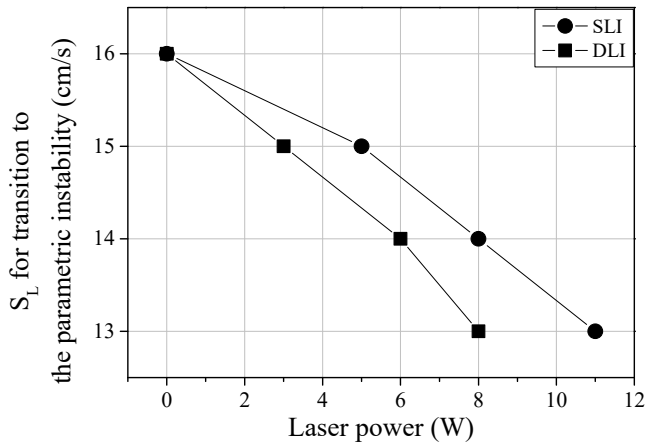

Fig. 6. Critical laser power required for the transition under various laminar burning velocities (mixture compositions are given in Table 1).

3.2. Correlation between the experimental result and theoretical velocity coupling mechanism

Searby and Rochwerger [3] presented a theoretical stability diagram for the transition from a flat flame to parametric instability in an acoustic field. They have shown that when the acoustic velocity

or pressure fluctuation amplitude reaches a critical value, parametric instability is generated at a certain wavenumber of the corrugated structure (at the onset of the transition, as shown in Fig. 3). In this work, a similar stability diagram was calculated for the flat flame at S_L = 16 cm/s, as shown in Fig. 7. The horizontal axis is the reduced wavenumber, kd, in which d = 0.0082 cm is the flame thickness ($d = D_{th}/S_L$ where D_{th} is the thermal diffusivity in the unburnt gas). The vertical axis is the reduced acoustic velocity, $u_a = U_a/S_L$, where U_a is the acoustic velocity in the unburnt gas. The measured wavenumber (see flame image of Regime III at t = 2.372 s from Fig.2) of the corrugated structure at the onset of the parametric instability, kd = 0.116, is close to the value shown in Fig. 7. With this understanding, the acoustic pressure fluctuation during laser-induced flame propagation is reviewed. Flames at S_L = 13 cm/s under critical laser powers of *SLI* – 11 W and *DLI* – 8 W are taken as a typical representation for conditions causing the transition by laser irradiation (transition conditions). These representative conditions are compared with the transition without laser irradiation at S_L = 16 cm/s and other non-transition conditions (S_L = 13 cm/s, *DLI* – 7 W and S_L =13 cm/s, 0 W without laser irradiation).

Figure 8 shows the time-dependent acoustic pressure fluctuation of propagating flames under the conditions mentioned above. The parametric instability represented by a sudden growth of acoustic pressure occurs after the primary acoustic instability. Only a truncated pressure history until the transition to parametric instability is shown in Fig. 8 to highlight the transition to parametric instability. In Fig. 8, parametric instability occurs at an almost similar acoustic pressure amplitude, which is approximately 0.4 kPa for all transition conditions. On the other hand, for S_L = 13 cm/s, a laser power of 7 W cannot induce the transition in the case of *DLI* as the acoustic pressure in the tube does not reach 0.4 kPa, but the laser irradiation effect is evident in the increased acoustic pressure compared to the case without laser irradiation for the same S_L = 13 cm/s (0 W). Hence, it is confirmed that the acoustic pressure needs to reach a critical value (0.4 kPa in this experiment) to generate a transition to parametric instability, as can be seen in the stability diagram in Fig. 7. In addition, the wavenumber of the corrugated structure found at the moment of the transition conditions in Fig. 8 is the same as that

found in Fig. 3, k = 14.1 cm^{-1}. This value is close to the one found in [4] and can be theoretically calculated using the presented method in their work.

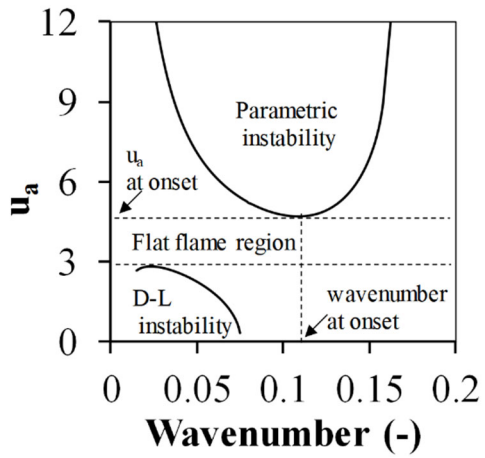

Fig. 7. Stability diagram at S_L = 16 cm/s for $C_2H_4/O_2/CO_2$ mixture with Le = 1.05.

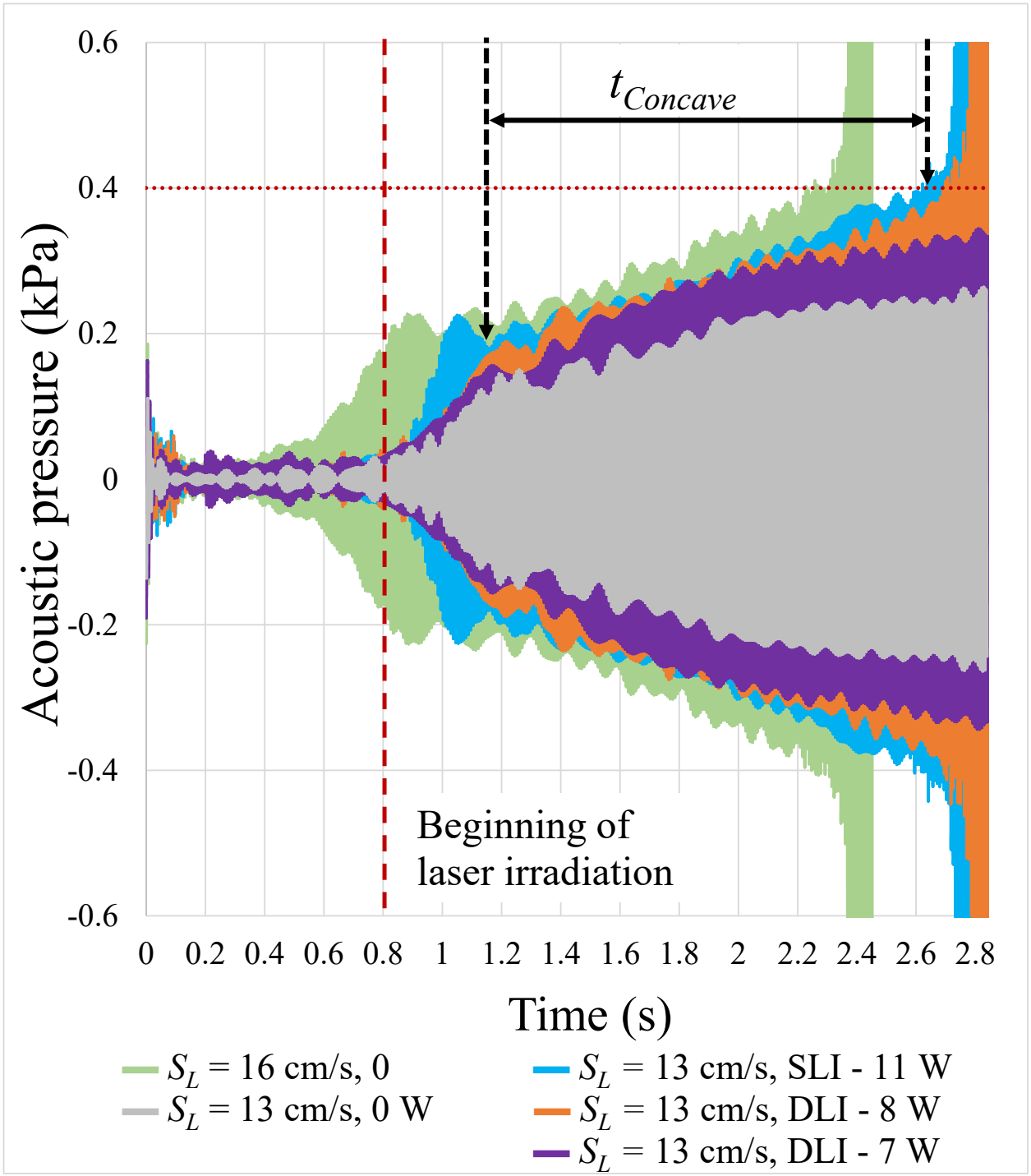

Fig. 8. Acoustic pressure fluctuation in the tube during flame propagation under various conditions (mixture compositions are given in Table 1).

Notably, the propagating flat flame at S_L = 13 cm/s without laser irradiation could not transition to parametric instability, as is evident from the pressure history shown in Fig. 8. However, when the circular portion(s) of the flat flame is modified to concave segment(s) (the wavelength of the concave structure is the diameter of the circular portion) using laser irradiation, the transition could occur. This

means the structural modification of the flame can trigger the emergence of the corrugated structure on the way to generate the transition (the area increase caused by the increase in tube diameter will not be effective in causing the transition as it changes acoustic losses as well as the initial growth rate of primary instability). However, a precise understanding of the relationship between laser-induced flame structures and the criteria of the transition is still obscure. This relationship can be clarified by investigating how the deformed flame in the case of *DLI* is more effective in deriving the transition than that in *SLI*.

To address this, we investigated the velocity coupling mechanism, which was first recognized by Markstein [22] who reported the effect of flame surface area variation on the generation of thermo-acoustic instability. The acoustic velocity in the tube modulates the total flame surface area fluctuation, which then modulates the heat release rate in phase with the acoustic pressure fluctuation and may lead to an enhancement in acoustic vibration [23]. Considering velocity coupling, Pelce and Rochwerger [10] performed a linear analysis for a weak cellular flame characterized by small amplitude sinusoidal cells, $ak \ll 1$, which is just above the planar flame stability threshold. They defined the transfer function, Tr, of the heat release rate to the acoustic velocity at the flame front to calculate the growth rate of acoustic instability driven by the effect of acoustic acceleration on the geometry of the flame front. The growth rate of the instability is given by [10]:

$$1/\tau = Im(Tr)G(r, \omega_n) \tag{3}$$

where $Im(Tr)$ is the imaginary part of Tr and $G(r, \omega_n)$ is the acoustic structure function of the relative flame position, r, of the flame in the tube and the resonant frequencies ω_n. $G(r, \omega_n)$ represents the normalized product of the acoustic pressure times the acoustic velocity at the flame front. In this analysis, they showed that the dimension of the cellular structure of the flame is an important factor in determining the growth of the instability. Tr was found to be proportional to $(ak)^2$; thus, the growth rate of the instability is proportional to $(ak)^2$. Clanet [11] extended the calculations performed by Pelce and Rochwerger and extrapolated them to an experimental configuration of nonlinear cells far from the planar flame stability limit. With the typical aspect ratio of the wrinkling, $ak \approx 0.5$, the growth rate

of thermo-acoustic instability predicted from the modified model agreed well with the experimental results of the gaseous flame (within a factor of 2).

The flame surface area in our work is controlled by laser irradiation; thus, we investigated the relation between $(ak)^2$ of the concave structure and the growth rate of the corresponding acoustic pressure fluctuation during the propagation period of the deformed concave flame at S_L = 13 cm/s. The growth rate is calculated by fitting pressure time series as follows:

$$A = A_0 e^{t/\tau} \tag{4}$$

where $1/\tau$ is the growth rate, A and A_0 are the final and initial amplitudes of acoustic pressures, and t is the time of the calculation period, which is defined from flame propagation videos and corresponds mostly to the relative stabilization period of primary acoustic instability. Precisely, the period starts from the moment after the initial growth period of primary acoustic instability (where the concave structure is fully developed) and ends with the appearance of the corrugated structure before transitioning to parametric instability. This period denoted by $t_{Concave}$ is shown in pressure history for S_L = 13 cm/s with a laser power of 11 W in the case of *SLI* (Fig. 8).

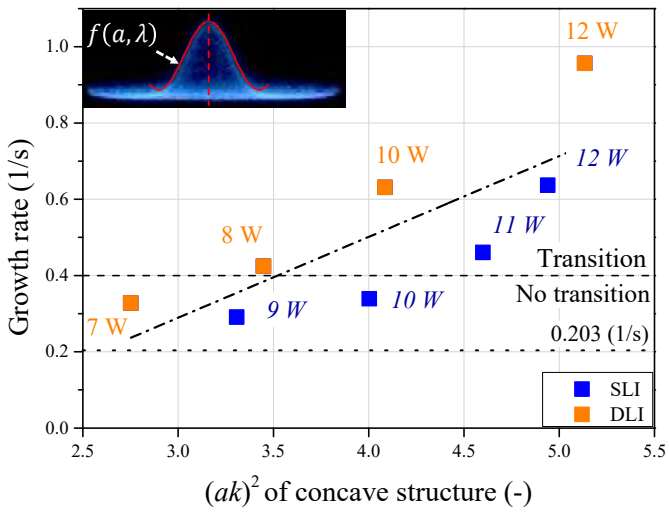

Fig. 9. Relationship between $(ak)^2$ of the concave structure and the growth rate of acoustic pressure fluctuation at S_L = 13 cm/s and Le = 1.05. The horizontal dotted line denotes the growth rate without laser irradiation. The horizontal dashed line denotes the critical growth rate (~ 0.400 1/s) to reach parametric instability.

Figure 9 shows the variation in growth rate during concave structure propagation with its geometric factor $(ak)^2$. The measurements of a and k were performed, assuming that the concave structure is the sinusoidal function of a and λ, as shown in the upper left corner of the figure. Flame propagation videos showed that after the concave structure was fully formed, k of the concave structure was almost constant during flame propagation. On the other hand, a of the concave structure fluctuated between the maximum and minimum in each cycle of flame oscillation. Accordingly, the horizontal axis in Fig. 9 presents $(ak)^2$ taken from the constant k and the averaged a of the maximum and minimum a. Moreover, $(ak)^2$ for *DLI* was calculated as the sum of the values for each cell of the double concave structure since each cell contributes to the total growth rate of the instability. It can be seen from Fig. 9 that the growth rate can be considered as a linear function of $(ak)^2$ if either *SLI* or *DLI* is considered separately. However, when both *SLI* and *DLI* experimental data are considered, an apparent discrepancy on the linear relationship between $(ak)^2$ and the growth rate can be observed. Moreover, $(ak)^2$ at transition is higher for *SLI* than that for *DLI*. Hence, $(ak)^2$ is not the criteria controlling the transition to parametric instability. The difference between this experimental result and the theoretical velocity coupling mechanism may be because cellular structures are assumed to be uniformly distributed over the flame front in the analysis of velocity coupling, while they are nonuniformly distributed and are limited in cell number in the experiments. Moreover, a larger aspect ratio, $ak \geq 1.1$, was obtained in the present work compared to that in the previous works [10,11]; thus, $ak \geq 1.1$ could also contribute to that difference.

3.3. Mechanism to enhance instability of laser-induced flame propagating under *SLI* and *DLI*

The conversion to the concave segment(s) from the circular portion(s) of the flat flame induced by laser irradiation increased the flame surface area. This increment could be attributed to the transition to parametric instability of the flame. Hence, to clarify the effect on the increase of the flame surface area, the correlation between the concave segment area and the growth rate of acoustic pressure was investigated. Only the area of the concave structure is considered because the planar segment of the deformed flame would limit any additional contribution to derive the transition.

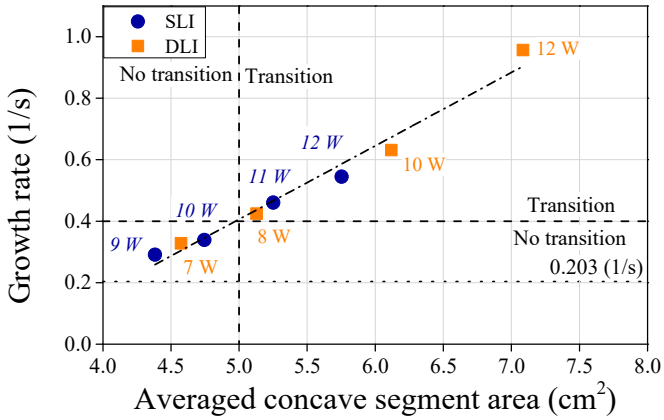

Fig. 10. Relationship between the concave segment area and the growth rate of acoustic pressure fluctuation at S_L = 13 cm/s and Le = 1.05. The horizontal dotted line denotes the growth rate without laser irradiation. The horizontal and vertical dashed lines denote the critical growth rate (~ 0.400 1/s) and critical average concave segment area (~ 5 cm^2), respectively, to reach parametric instability.

Figure 10 shows the variation in the growth rate of acoustic pressure with the measured average concave segment area. The horizontal axis presents the average area taken from the maximum and minimum areas of the concave segment during flame propagation. The growth rate of the propagating flat flame without laser irradiation at S_L = 13 cm/s was 0.203 (1/s), as shown by a dotted horizontal line in Figs. 9 and 10; thus, the growth rate increases with laser irradiation. From Fig. 10, we found that a linear relationship exists between the concave segment area and the growth rate of the acoustic pressure, indicating that an increase in the flame area causes a linear increase in the growth rate of pressure fluctuation. Thus, a larger growth rate means a higher potential for pressure fluctuation amplitude to reach the critical value of 0.4 kPa to generate the transition. The growth rate in Fig. 9 is nearly an order of magnitude smaller than typical velocity coupling predictions [11] because the flame is in the flat flame region, as illustrated in Fig. 7, where area fluctuation is suppressed due to the stability of a planar flame front. Recall that the transition of flames at S_L = 13 cm/s occurs at laser powers of 11 W and 8 W for *SLI* and *DLI*, respectively. Therefore, the graph in Fig. 10 is separated into transition region and no-transition region with a threshold growth rate for the transition to parametric instability of ~0.4 (1/s) and a corresponding concave segment area threshold of ~5 cm^2. Next, compared to *SLI* at the same laser power, *DLI* developed a larger concave segment area

corresponding to a greater growth rate of pressure fluctuation, so the flames under *DLI* need a smaller laser power to meet the transition criteria. This is why *DLI* is more effective than *SLI* in initiating the transition to parametric instability.

The concave segment area of the deformed flame in Fig. 10 relies on a and λ of the concave structure. Subsequently, its area is calculated using the surface of revolution method. Figure 11 shows the average values of a and λ of concave structures induced by *SLI* and *DLI* at S_L = 13 cm/s. Under the same total laser power supply, the total power of *SLI* is twice that of the individual laser beam of *DLI*. However, the experimental results show that both a and λ of the deformed concave structure induced by *DLI* are larger than half of those induced by *SLI*, as shown in Fig. 11. Thus, a larger area is deformed by *DLI* than that by *SLI* and could be the reason why *DLI* is more efficient than *SLI* in inducing the transition to parametric instability.

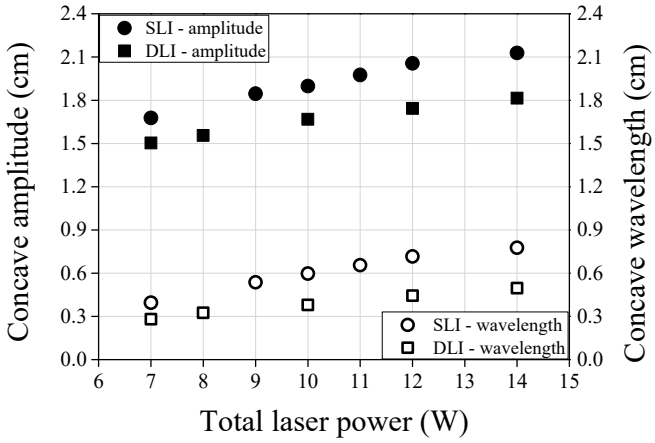

Fig. 11. Amplitude and wavelength of concave structures induced by *SLI* and *DLI* at S_L = 13 cm/s.

In an earlier work [18], the laser-induced flame could generate the transition in a structure (either concave or convex) depending on whether *Le* is larger or smaller than unity, respectively. To clarify the reliability of the above discussion on the importance of the deformed area on the transition criteria, additional experiments were conducted for a gas mixture with *Le* = 0.8 at S_L = 12 cm/s (mixture composition is shown in Table 2). In this low-*Le* experiment, the transition to parametric instability occurred only from the deformed convex structure induced via *SLI*. Interestingly, *DLI*, which was more effective than *SLI* in causing instability for the flame with *Le* > 1, was not effective for the flame with *Le* < 1. Figure 12 shows the correlation between the area of the convex structure and the growth

rate of acoustic pressure fluctuation during the structure's propagation period. The growth rate is calculated using Eq. (4) with t starting from the emerging moment of the convex structure until the structure reaches the maximum elongation (noted as t_{convex} in Fig. 2). An example is shown at 10 W under *SLI* in Fig. 11. The average area of the convex structure, $\bar{S}$, during the calculated period is shown in the horizontal axis of Fig. 11 and is calculated as follows:

$$\bar{S} = \frac{1}{t}\int_0^t S dt \tag{5}$$

Similar to the case for $Le > 1$ (Fig. 10), a linear relationship between the convex area induced by *SLI* and *DLI* and the growth rate is found for $Le < 1$ (Fig. 12). Figure 12 shows that the double convex structures induced by *DLI* have smaller areas than single convex structures induced by *SLI* at the same total laser power. Moreover, only the deformed convex structures under *SLI* with a total laser power of more than 10 W can generate the transition. Here, the threshold growth rate and the convex area were approximately 13 1/s and 20 cm^2, respectively. Figure 13 shows that the increasing convex area during t_{convex} for 10 W under *SLI* enhances the growth of acoustic pressure fluctuation, which further generates the transition at a laser power of 10 W under *SLI*. As a comparison, two other cases shown in Fig. 13 (10 W – *DLI* and 0 W) did not have a larger convex area and consequently a larger pressure growth that can induce instability. Moreover, for the condition of 10 W – *DLI*, the convex structure, after reaching a maximum area, is gradually diminished, and the concave structure is subsequently developed. Accordingly, *SLI* is more effective than *DLI* in deriving transition from the convex structure with $Le < 1$. Hence, area modification caused by laser irradiation is the determining factor for the generation of parametric instability.

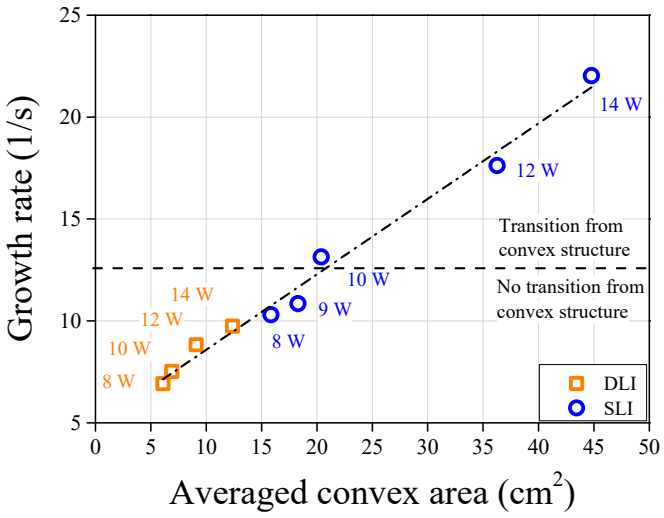

Fig. 12. Relationship between the deformed convex area and the growth rate of acoustic pressure fluctuation at S_L = 12 cm/s and Le = 0.8.

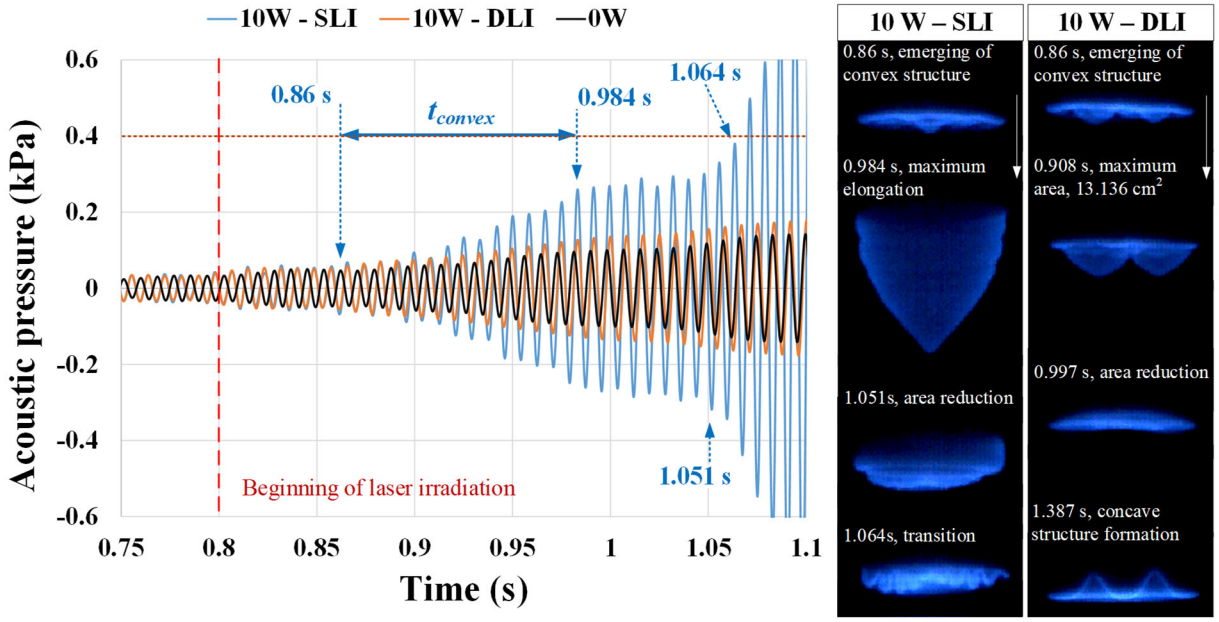

Fig 13. Comparison of the growth of the acoustic pressure fluctuation under no laser, *SLI*, and *DLI* for S_L = 12 cm/s and Le = 0.8.

4. Conclusion

We modified the existing *SLI* setup to establish a new *DLI* approach that can form double cellular structures, while *SLI* only forms single cellular structures. A comprehensive criterion of the transition from primary acoustic instability to parametric instability was investigated under these two laser irradiation conditions. It was found that *DLI* is more effective than *SLI* in driving the transition to

parametric instability under same total laser power. The results showed that the growth rate of primary acoustic instability during the propagation of the deformed flame is important to enhance the pressure fluctuation amplitude that further reaches the critical value for the transition to parametric instability. More importantly, $(ak)^2$ of the cell deformed on the flame does not provide a comprehensive transition criterion, as mentioned in the original theory of velocity coupling. Possibly, $(ak)^2$ does not represent the increase in flame area due to the nonuniform deformation of the flame structure; thus, it cannot be correlated with the growth rate across both *SLI* and *DLI* experiments. On the other hand, the measured flame area correlated well with the growth rates. Using the *DLI* method, we proved that the actual flame area, rather than $(ak)^2$, determines the growth rate under nonhomogeneous cell distribution.

Acknowledgment

This study is carried out under the support of a Grant-in-Aid for Scientific Research (KIBAN(A)#18H03755) from MEXT Japan.

References

[1] J. Rayleigh, The explanation of certain acoustical phenomena, Nature 18 (1878) 319–321.

[2] G. Searby, Acoustic instability in premixed flames, Combust. Sci. Technol. 81 (1992) 221–231.

[3] G. Searby, D. Rochwerger, A parametric acoustic instability in premixed flame, J. Fluid Mech. 231 (1991) 529–543.

[4] A.K. Dubey, Y. Koyama, S.H. Yoon, N. Hashimoto, O. Fujita, Range of "complete" instability of flat flames propagating downward in the acoustic field in combustion tube: Lewis number effect, Combust. Flame 216 (2020) 326-337.

[5] V. Vaezi, R.C. Aldredge, Laminar-flame instabilities in a taylor-couette combustor, Combust. Flame 121 (2000) 356–366.

[6] R.C. Aldredge, N.J. Killingsworth, Experimental evaluation of Markstein-number influence on thermoacoustic instability, Combust. Flame 137 (2004) 178–197.

[7] A.K. Dubey, Y. Koyama, N. Hashimoto, O. Fujita, Effect of geometrical parameters on thermo-acoustic instability of downward propagating flames in tubes, Proc. Combust. Inst. 2 (2019) 1869-1877.

[8] A.K. Dubey, Y. Koyama, N. Hashimoto, O. Fujita, Exploring a critical diameter for thermo-acoustic instability of downward propagating flames in tubes, doi.org/10.1016/j.proci.2020.06.018.

[9] A.K. Dubey, Y. Koyama, N. Hashimoto, O. Fujita, Experimental and theoretical study of secondary acoustic instability of downward propagating flames: Higher modes and growth rates, Combust. Flame 205 (2019) 316–326.

[10] P. Pelcé, D. Rochwerger, Vibratory instability of cellular flames propagating in tubes, J. Fluid Mech. 239 (1992) 293–307.

[11] C. Clanet, G. Searby, P. Clavin, Primary acoustic instability of flames propagating in tubes: cases of spray and premixed gas combustion, J. Fluid Mech. 385 (1999) 157–197.

[12] S.H. Yoon, T.J. Noh, O. Fujita, Onset mechanism of primary acoustic instability in downward-propagating flames, Combust. Flame 170 (2016) 1–11.

[13] M. Tsuchimoto, O. Fujita, T. Honko, Y. Nakamura, H. Ito, Research on the relation of flame front curvature and oscillatory flame propagation by external laser irradiation method, Proc. Combust. Inst. 32 (2009) 1003–1007.

[14] S.H. Yoon, T.J. Noh, O. Fujita, Effects of Lewis number on generation of primary acoustic instability in downward-propagating flames, Proc. Combust. Inst. 36 (2017) 1603–1611.

[15] S.H. Yoon, L. Hu, O. Fujita, Experimental observation of pulsating instability under acoustic field in downward-propagating flames at large Lewis number, Combust. Flame 188 (2018) 1-4.

[16] J.S. Park, O. Fujita, Y. Nakamura, H. Ito, Transition of flat flames to turbulent motion induced by external laser irradiation, Proc. Combust. Inst. 33 (2011) 1105–1112.

[17] Y. Taniyama, O. Fujita, Initiation and formation of the corrugated structure leading to the selfturbulization of downward propagating flames in a combustion tube with external laser absorption, Combust. Flame 161 (2014) 1558–1565.

[18] Y. Chung, O. Fujita, N. Hashimoto, Effect of Le on criteria of transition to secondary acoustic instability of downward-propagating flame in a tube with controlled curvature induced by external laser, Proc. Combust. Inst. 37 (2019) 1887–1894.

[19] R.J. Kee, R.M. Rupley, et al., CHEMKIN PRO, Reaction Design, Inc., San Diego, CA, 2009.

[20] The National Institute of Standards and Technology (NIST), available at http://webbook.nist.gov/chemistry.

[21] K. Aguilar, Y. Taniyama, H. Ito, O. Fujita, Interaction Between Propagation Speed and Flame Structure in Downward Cellular Propagating Flame in a Combustion Tube with Co2 Laser Irradiation, Combust. Sci. Technol. 186 (2014) 1434–1446.

[22] G.H. Markstein, Flames as amplifiers of fluid mechanical disturbances, Proceedings of the 6th National Congress for Applied Mechanics, Cambridge, 1970, pp. 11–33.

[23] J. Jarosinski, B. Veyssiere, Combustion Phenomena: Selected Mechanisms of Flame Formation, Propagation and Extinction, CRC Press, 2009, pp.76–77.